Journal of Materials Chemistry A

Accepted Manuscript

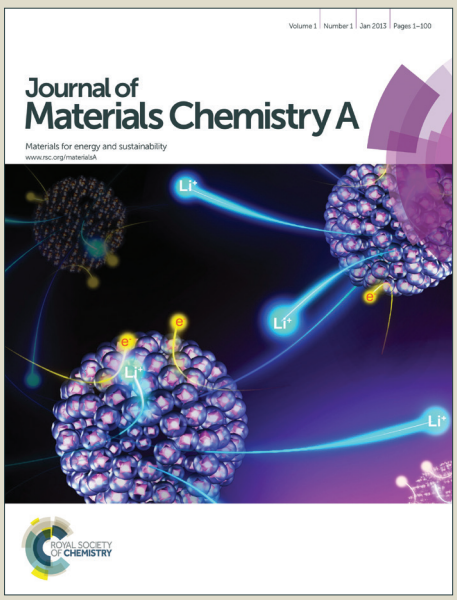

ROYAL SOCIETY OF CHEMISTRY

www.rsc.org/materialsA

Journal of Materials Chemistry A

ARTICLE

Mechanisms of methane decomposition and carbon species oxidation on $Pr_{0.42}Sr_{0.6}Co_{0.2}Fe_{0.7}Nb_{0.1}O_{3-\sigma}$ electrode with high catalytic activity

Received 00th January 20xx,
Accepted 00th January 20xx

DOI: 10.1039/x0xx00000x

www.rsc.org/

Peng Zhang,[a] Guoqing Guan,*[ab] Deni S. Khaerudini,[a] Xiaogang Hao,[c] Chunfeng Xue,[c] Minfang Han,[d] Yutaka Kasai[e] and Abuliti Abudula,[ab]

Carbon deposition on $Pr_{0.42}Sr_{0.6}Co_{0.2}Fe_{0.7}Nb_{0.1}O_{3-\sigma}$ (PSCFN) and Ni-yttria stabilized zirconia (Ni-YSZ) due to thermal CH_4 decomposition under dry CH_4 has been investigated by temperature-programmed reaction techniques. The morphologies of carbon formed are characterized by using scanning electron microscopy (SEM). It is found that carbon nanofibers are obviously formed on PSCFN while spherical carbons formed on Ni-YSZ. Analyses of the results on CH_4 temperature-programmed decomposition and O_2 temperature-programmed oxidation reveal that the high catalytic activity of cracking CH_4 and the easier oxidation of the generated carbon species on PSCFN could be the main reason why PSCFN shows high performance and good stability in direct CH_4 fueled solid oxide fuel cells (SOFCs).

Introduction

Solid oxide fuel cells (SOFCs) technology is suggested to play a critical role in both our current and future energy solutions owing to the advantages of the most efficiency for the generation of electricity, fuel flexibility, low emissions and so on.[1-4] Hydrocarbon, especially methane, is a promising fuel for SOFCs to replace the pure hydrogen for the low cost and wide applications.[5-7] Recently, many interests have been given to the tolerance of SOFC anodes to direct conversion of dry hydrocarbon fuels.[8-11] Here, "direct conversion" means conversion in the SOFC without pre-mixing the fuel gas with steam or CO_2, and without processing the fuel before it enters the cell stack, which was defined by Mogensen and Kammer.[12] Therefore, direct conversion only concludes electrochemical oxidation of the fuel and/or thermal cracking of the products. Based on the operating principle of direct hydrocarbon SOFC, the oxygen molecules are reduced to oxygen ions at the cathode, as driven by the electrochemical potential difference between anode and cathode, the oxygen ions will be electrochemically oxidized at the anode with the fuels diffused through the porous structure. The overall reaction in the anode side can be expressed as:

$$C_nH_{2n+2} + (3n+1)O^{2-} \rightarrow \mathrm{nCO_2} + (n+1)H_2O + (6n+2)e^- \quad (1)$$

Murray et al.[13] investigated the direct-methane SOFC with a ceria-based anode, and concluded that the direct electrochemical oxidation of methane, as shown in the following equation (2), is the primary anode reaction.

$$CH_4 + 4O^{2-} \rightarrow CO_2 + 2H_2O + 8e^- \quad (2)$$

Part et al.[14] also reported on the direct, electrochemical oxidation of various hydrocarbons (methane, ethane, 1-butene, n-butane and toluene) with a composite anode of copper and ceria. Huang et al.[15] developed a double perovskite anode of $Sr_2MgMoO_{6-\sigma}$, and considered that the dry methane can directly be converted by electrochemical oxidation on the anode through the equation (2). However, Mogensen and Kammer[12] argued that reaction (2) is highly unlikely to occur in one step. Instead, the reactions with methane as the fuel may proceed via the following steps:

$$\mathrm{CH_4} + O^{2-} \rightarrow CH_3OH + 2e^- \quad (3)$$

$$CH_3OH + 2O^{2-} \rightarrow HCOOH + H_2O + 4e^- \quad (4)$$

$$\mathrm{HCOOH} + O^{2-} \rightarrow CO_2 + H_2O + 2e^- \quad (5)$$

Cracking of methane followed by electrochemical oxidation of the cracking products proceeds as follows

$$C_xH_y \rightarrow xC + \frac{y}{2}H_2 \quad (6)$$

$$C + 2O^{2-} \rightarrow CO_2 + 4e^- \quad (7)$$

$$H_2 + O^{2-} \rightarrow H_2O + 2e^- \quad (8)$$

Fisher II et al.[16] used LSCF as the anode and suggested that the catalytic activity for the direct electrochemical oxidation of CH_4 to produce CO_2 via (i) CH_4 decomposition, (ii) electrochemical oxidation of hydrogen, and (iii) electrochemical oxidation of carbon to CO_2 or CO. Sun et al.[17] also investigated the carbon deposition behaviour on $La_{0.4}Sr_{0.5}Ba_{0.1}TiO_3$ anode catalyst. As we known, the conventional Ni-based cermet anode in SOFCs shows a weak coking tolerance in hydrocarbon fuels, which hinders it further commercial

[a] Graduate School of Science and Technology, Hirosaki University, 1-bunkyocho, Hirosaki 036-8560, Japan.
[b] North Japan Research Institute for Sustainable Energy (NJRISE), Hirosaki University, 2-1-3 Matsubara, Aomori 030-0813, Japan. Tel.: +81-17-762-7756; fax: +81-17-735-5411, E-mail: guan@hirosaki-u.ac.jp
[c] Department of Chemical Engineering, Taiyuan University of Technology, Taiyuan 030024, China.
[d] Department of Thermal Engineering, Tsinghua University, Beijing, 100084, PR China.
[e] Industrial Research Institute, Aomori Prefectural Industrial Technology Research Center, 4-11-6, Second Tonyamachi, Aomori 030-0113, Japan

utilization.[18-20] Instead, the perovskite oxides have been widely used as the anode material for SOFCs owing to their good structural and chemical stability in carbon-contained fuels.[13,21-23] Recently, our and other groups have shown that $Pr_xSr_{0.6}Co_{0.2}Fe_{0.7}Nb_{0.1}O_{3-\sigma}$ can be effectively employed as an anode for the direct methane fuel SOFCs.[24-26] So far, the coking tolerance mechanism is still not so clear for this kind of oxide anode, and only a few of studies investigated the oxidation behaviours of carbon species on the anode. Especially, recent studies on carbon growth on the oxide electrodes revealed that the carbon deposition should be from methane decomposition when using the pure oxides, such as YSZ and Y_2O_3.[27] As such, it is interesting to study in details whether the carbon deposits or not and what kind of carbon species will be formed on the PSCFN anode. Based on those previous studies, the purpose of this study is to investigate the methane dissociation and carbon deposition capability on the PSCFN anode in comparison to the conventional Ni-YSZ anode. A set of different characterization methods, including temperature-programmed cracking reaction (TPCR), temperature-programmed oxidation (TPO), thermogravimetric (TG) and scanning electron micrographs (SEM) were applied to investigate the carbon species formed on PSCFN and Ni-YSZ materials.

Experimental

Sample fabrication

$Pr_{0.42}Sr_{0.6}Co_{0.2}Fe_{0.7}Nb_{0.1}O_{3-\sigma}$ (PSCFN) perovskite oxides were prepared by solid-state reaction from the materials with high purity: $Pr(NO_3)_3{\cdot}6H_2O$, $SrCO_3$, $Co(NO_3)_2{\cdot}6H_2O$, Fe_2O_3 and MoO_3 (99.9% Wako, Japan).[25] These materials were mixed by ball milling. The calcinations of the precursor powders were performed at 1050 ^{o}C for 5 h in air to obtain a pure phase. The commercially available powders, NiO (Soekawa Chemicals, Japan) and YSZ (Tosoh Corporation, Japan) were used for comparison.

Material characterization

Methane temperature-programmed cracking reaction (CH_4-TPCR) was performed to identify the methane cracking behaviour. Both of NiO-YSZ (weight ratio, 50:50) and PSCFN powders were ball milled for 6 h, respectively, and sieved into the particle range of 30 to 60 mesh. Approximately 0.1 g of sample was placed in a U-type quartz reactor. The sample was reduced in 5% H_2 +95% Ar (total 50 ml min^{-1}) at 900 ^{o}C for 1 h, after cooling in Ar, the reactor was programmatically heated from 50 to 900 ^{o}C at 10 ^{o}C min^{-1} or kept at 700, 800, 850 and 900 ^{o}C for 30 min and 850 ^{o}C for 600 min, respectively, under pure CH_4 with a flow rate of 30 cm^3 min^{-1}. The consumption of methane was monitored by an in-situ thermal conductivity detector (TCD).

The temperature-programmed oxidation (TPO) method was employed to characterize the carbon formed on the anode materials, the reaction products were analyzed by a BEC mass spectrum S/N0107. Approximately 0.1 g of coked sample was put in a U-type quartz tube that was loaded into the TPO apparatus and exposed to a pure O_2 flow at 20 ml min^{-1}. The temperature was then increased from room temperature to 900^{o}C at 10 ^{o}C min^{-1}.

To examine the amount of deposited carbon on both Ni-YSZ and PSCFN samples. Approximately 0.01 g of sample was loaded in an alumina crucible and tested by thermogravimetric (TG)/differential thermal analysis (DTA; DTG-60H, Shimadzu, Japan). The sample wa heated in air from room temperature to 900 ^{o}C at a heating rate of 10 ^{o}C min^{-1}.

Crystallographic phases of Ni-YSZ and PSCFN samples were carried out using X-ray diffraction (XRD, Shimadazu, Japan) with Cu-Kα radiation. The morphologies of samples after each operation were investigated by scanning electron microscopy (SEM, Hitachi, Japan) with an Energy Dispersive X-ray Detector (EDX).

Results and discussion

Carbon deposition

Rapid degradation behaviour is frequently observed for the SOFC with the Ni-based anode when methane is used as fuel, because the good catalytic activity of Ni for the cracking of methane results in the carbon depositing on the active sites of the Ni catalyst.[20,28] In contrast, the good stability was proved for PSCFN anode in direct methane fuelled SOFC,[24] but whether the carbon deposition appeared on PSCFN anode as an intermediate step or not is still not clarified. Herein, the carbon deposition behaviours of both Ni-YSZ and PSCFN catalysts were investigated by treating them in pure methane from 50 to 900 ^{o}C with a heating rate of 10 ^{o}C min^{-1}. Fig. 1 shows the CH_4-TPCR results of both Ni-YSZ and PSCFN samples. It can be seen that CH_4 decomposition on both PSCFN and Ni-YSZ started at about 580 ^{o}C. Ni-YSZ sample presented a continuously consuming of CH_4 until the end of investigation. In contrast, for PSCFN, the CH_4 decomposition peak reached the maximum value at 840 ^{o}C, and then the decomposition declined quickly and stopped at about 900 ^{o}C. Also the consumption rate of methane in PSCFN is much faster than that in Ni-YSZ sample, indicating a fast cracking methane property for PSCFN catalyst. Such methane decomposition behaviour on PSCFN may attribute to the generation of nano CoFe-alloy after it is reduced in H_2, as reported in our previous work[25] and Yang et al.[24]. Moreover, the decline of methane cracking on PSCFN may due to the coverage of carbon on the surface of CoFe-alloy when the temperature was increased higher than 840 ^{o}C. To prove

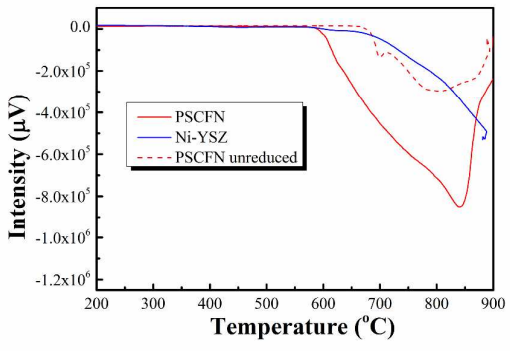

Fig. 1 Profiles of CH_4 temperature-programmed decomposition on PSCFN and Ni-YSZ samples.

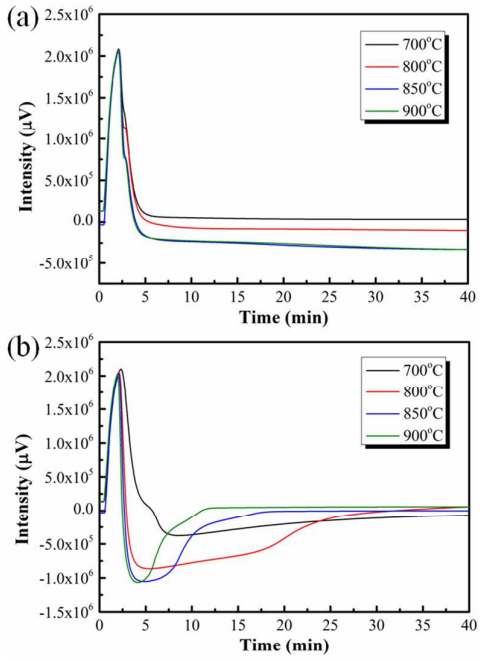

Fig. 2 Profiles of CH_4 temperature-programmed decomposition at different temperatures for 30 min on Ni-YSZ (a) and PSCFN (b).

that the methane cracking on PSCFN is promoted by the formation of nano CoFe-alloy, the CH_4-TPCR test with an unreduced PSCFN sample was also performed and the results are shown with the dash line in Fig. 1. One can see that the starting temperature of CH_4 consuming from 580 °C increased to about 670 °C, which may be caused by the reducing of PSCFN in CH_4, and then a similar CH_4 decomposition behaviour appeared as that obtained on the reduced PSCFN sample by further increasing the temperature higher than 720 °C.

The properties of CH_4-TPCR on Ni-YSZ and PSCFN at different temperatures are aslo investigated. The results are shown in Fig. 2. From Fig. 2(a), the similar continuous consuming of CH_4 are observed at all temperatures for the Ni-YSZ sample. It can be seen that CH_4 cracking rate increases with the increase of reaction tempearture from 700 to 850 °C, and then keeps stable for further increasing temperature from 850 to 900 °C. For the PSCFN sample, as shown in Fig. 2(b), one can see that CH_4 cracks at first and then this cracking process stops after few minutes at all temperatures. The only difference of CH_4 cracking reactions at different temperatures is the cracking time, which decreases with the increase in the reaction temperature since the higher catalytic activity for CH_4 cracking at higher temperture.

Oxidation of carbon species

The activity of carbon species deposited on the anode was evaluated by temperature-programmed reaction with O_2. Prior to oxidation, both Ni-YSZ and PSCFN were reduced in 5% H_2/Ar at 900 °C for 45 min and then heat-treated in methane at 850 °C for 10 min. Fig. 3(a) and 3(b) show the MS-signal of effluent gas in CH_4 decomposition process. For PSCFN sample, the rate of CH_4

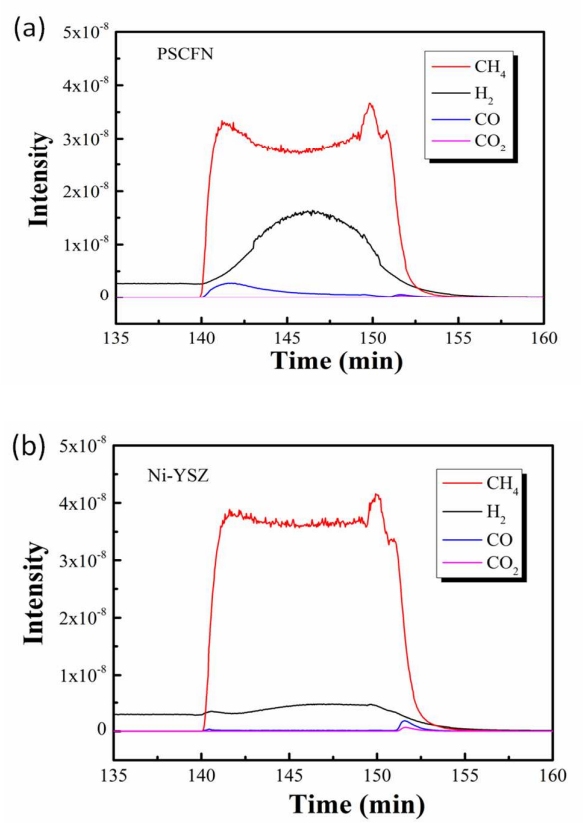

Fig. 3 MS-signals of effluent gas in CH_4 decomposition on (a) PSCFN and (b) Ni-YSZ at 850 °C.

decomposition gradually increased at first 7 min, and then the consumption of CH_4 slightly decreased with the increase in the decomposition time. Simultaneously, the amount of produced H_2 increased first and then decreased after the operation was performed for 7 min. In contrast, for Ni-YSZ sample, as shown in Fig. 3(b), a continuous increase of CH_4 decomposition was observed and a tiny of H_2 produced in this process. These results also showed that PSCFN is a more active catalyst than Ni-YSZ in cracking CH_4. In addition, from Fig. 3(a), a small amount of CO was generated at the beginning of CH_4 consumption stage, which should contribute to the highly reactive lattice oxygen in PSCFN sample, while almost no CO was observed over Ni-YSZ catalyst, as shown in Fig. 3(b).

In the fuel side of SOFC, carbon is generally oxidized by O^{2-} ions, which have higher catalytic activity than O_2 molecule. As such, the temperatures for the oxidation of carbon species by O_2 molecules on either Ni-YSZ or PSCFN sample should also be enough for the oxidation of carbon species by O^{2-} ions. The purposes of this study are to investigate CH_4 cracking behaviours on Ni-YSZ as well as PSCFN, and try to understand whether the properties of deposited carbons on Ni-YSZ and PSCFN are different or not. In our previous study [25], PSCFN material was applied as the symmetrical electrodes for SOFCs, in which PSCFN was used in both anode and cathode. In this case, even if the coking is formed on the PSCFN electrode in the fuel side, the gas flow to the anode can be changed to the cathode side. As such, the deposited carbon species can be reacted with O_2 directly and moved out from the electrode. Fig. 4

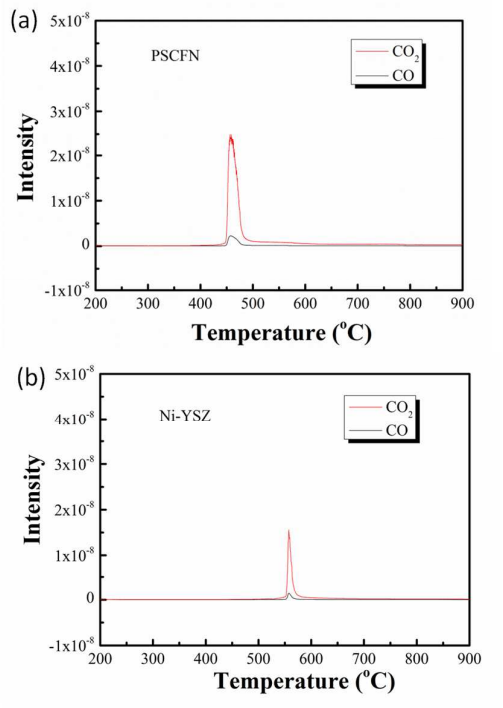

Fig. 4 MS-signals of effluent gas in O_2-TPO process on (a) PSCFN and (b) Ni-YSZ after CH_4 decomposition at 850 °C for 10 min.

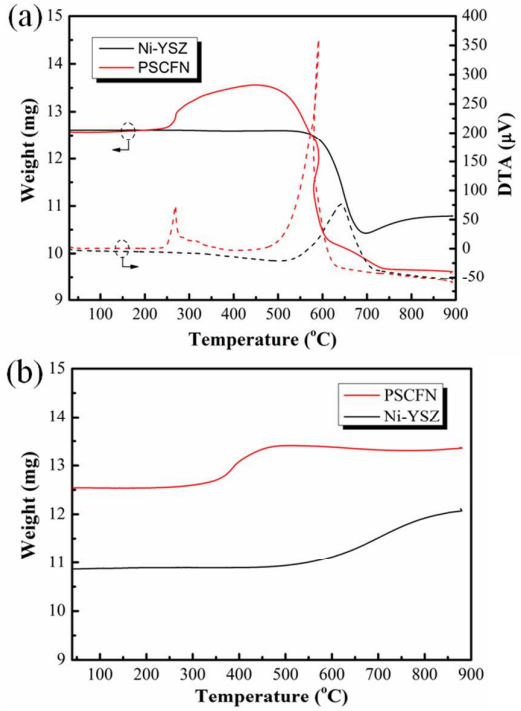

Fig. 5 TG/DTA curves of the Ni-YSZ and PSCFN samples after (a) carbon deposition in CH_4 at 850 °C and (b) reduced in H_2 at 900 °C.

shows MS-signals of outlet gas in O_2-TPO processes of Ni-YSZ and PSCFN after CH_4 was decomposed at 850 °C for 10 min. As shown in Fig. 4, the starting temperature of carbon oxidation on Ni-YSZ sample is about 540 °C and ended at around 610 °C with apparent peak at 556 °C, which is similar with other reported results.[29] While for PSCFN sample, the initiation temperature significantly decreased to 430 °C, which indicates that different types of carbonaceous species were formed on Ni-YSZ and PSCFN samples. One can see that the catalytic activity of the carbon species produced on PSCFN sample is much higher than that on Ni-YSZ owing to the lower reaction temperature with oxygen. Also the amount of deposited carbon species on the former is larger than that on the latter, which is consistent with the results shown in Figs. 1 and 3. Mogensen et al.[10] pointed out that the cracking of CH_4 followed by the electrochemical conversion of the cracking products demands that the anode is not only highly active for the cracking of CH_4 but also active for the oxidation of the cracking products. Therefore, the high catalytic activity for the cracking of CH_4 as well as the oxidation of the generated carbon on the PSCFN anode could be the main reason for its high performance and stability in direct CH_4 fuelled SOFCs.[24] TPO experiment is difficult to directly investigate the carbon species reacting with O^{2-} ions. Here, we did addition experiments, in which we simulated the real SOFC condition to investigate the oxidation behaviour of the carbon species on PSCFN by O^{2-} ions. As shown in Fig. S1, it can be seen that the carbon species on PSCFN can be also eliminated by the O^{2-} ions as we thought.

TG analysis

TG/DTA analysis was carried out to examine the thermal behaviour of the deposited carbon on both PSCFN and Ni-YSZ samples. As shown in Fig. 5(a), for the Ni-YSZ sample, the TG curve shows one weight loss, which starting at around 530 °C and ending at 700 °C, following a slight weight increase by further increasing temperature. The weight loss ratio is about 17.2%, which is related to the carbon burning process, and the increasing of the weight after 700 °C may be caused by the oxidation of the Ni, which also observed in the Fig. 5(b), which shows the TG results of Ni-YSZ and PSCFN sample in air after pre-treated in H_2 at 900 °C. In contrast, for the PSCFN sample, as shown in Fig. 5(a), there is a weight increase at the low temperature range from 220 to 430 °C, which may attribute to the oxidation of the nano CoFe-alloy, as presented similar curve at the temperature range from 220 to 450 °C in Fig. 5(b). By further increasing the temperature to 430 °C, there is a sharp weight loss for PSCFN sample, corresponds to a significantly peak of DTA curve, which may be caused by the firing of the deposited carbon. The amount of the weight loss in this process is about 30.9%, which is much higher than that for the Ni-YSZ sample. As for the fluctuation of the TG and DTA curves of PSCFN sample in the temperature range from 550 to 600 °C, as shown in Fig. 5(a), it is possible that the release of the heat in the rapid burning process of the special carbon species formed on PSCFN sample. Fig. 6 shows TG curves of Ni-YSZ and PSCFN samples after carbon deposition in pure CH_4 at 700, 850 and 900 °C, respectively. From Fig. 6(a), one can see that the weight decrease for Ni-YSZ sample exposed in CH_4 at 700 °C is only 0.6%, which is much less than 17% and 21% for the samples exposed at 850 and 900 °C, respectively. However, the starting temperature of the weight decrease, corresponding to the carbon

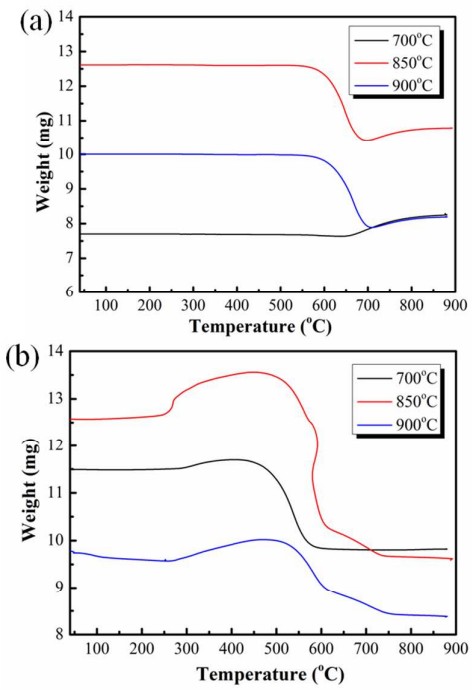

Fig. 6 TG curves of Ni-YSZ (a) and PSCFN (b) samples after carbon deposition in pure CH_4 at 700, 850 and 900 °C.

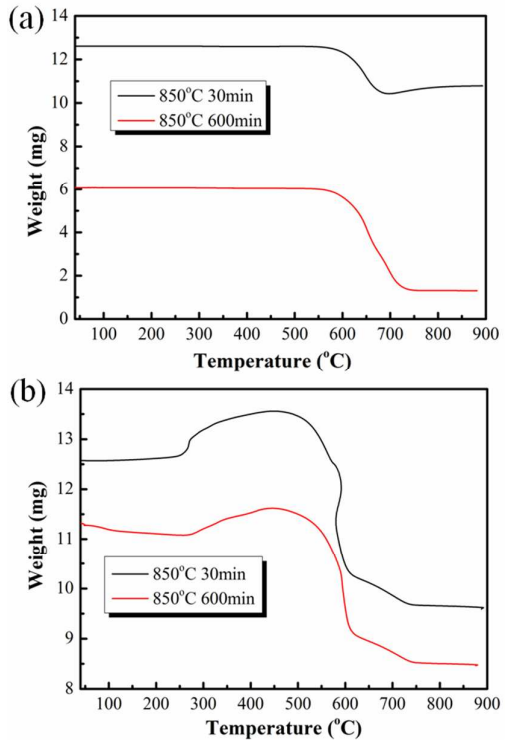

Fig. 7 TG curves of Ni-YSZ (a) and PSCFN (b) samples after carbon deposition in CH_4 at 850 °C for 30 and 600 min.

burnt, is almost the same for each sample. TG results of the deposited carbon on PSCFN sample are shown in Fig. 6(b). It can be seen that three curves show the similar tendency, in which a weight increase starts at about 250 °C and a weight decrease occurs from 425-475 °C. Fig. 7 shows TG curves of Ni-YSZ and PSCFN samples after carbon depositions in CH_4 at 850 °C for 30 and 600 min. One can see that there is no difference for the staring temperature of carbon species oxidation on both Ni-YSZ and PSCFN samples. The only difference for Ni-YSZ sample for 30 and 600 min is the weight loss ratio, as shown in the Fig. 7(a). The weight decrease amounts in the range of 550-750°C are 10 % and 75% when heat-treated in CH_4 at 850 °C for 30 and 600 min, respectively. From Fig. 7(b), it can be seen that the starting temperatures of the weight increase and decrease are the same when PSCFN samples are heat-treated in CH_4 for 30 and 600 min, respectively. Further, the values of both weight increase and decrease are also similar for the two samples, which are consistent with the results of CH_4-TPCR process. These results indicate that the carbon species generated on PSCFN sample has much higher catalytic activity for oxidization when comparing with that produced on the Ni-YSZ sample.

XRD patterns and microstructural characterization

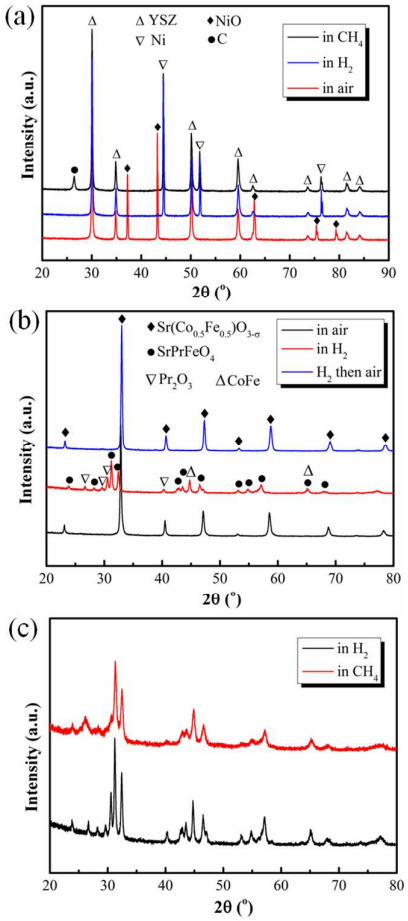

Fig. 8 XRD of Ni-YSZ sample after sintered in air, H_2 and CH_4 (a); XRD of PSCFN sample after sintered in air and H_2 (b); in H_2 and CH_4 (c).

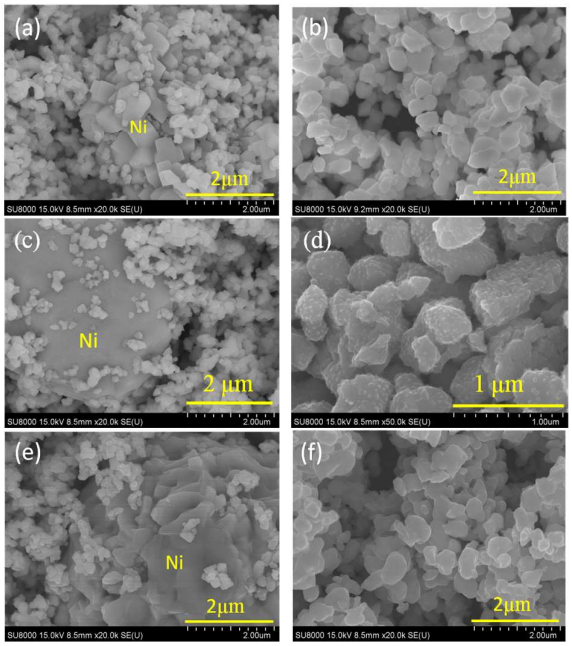

Fig. 9 Typical SEM images of (a) Ni-YSZ and (b) PSCFN fresh sample; (c) Ni-YSZ and (d) PSCFN after reduced in H_2 at 900 ^{o}C; (e) Ni-YSZ and (f) PSCFN after O_2-TPO test.

The phase structures of Ni-YSZ and PSCFN are shown in Fig. 8. From Fig. 8(a), one can see that NiO phase is converted to Ni phase after NiO-YSZ is reduced in H_2 at 900 ^{o}C. Carbon phase at the peak of 2θ = 26.4^{o} is observed after Ni-YSZ is heat-treated in CH_4 at 900 ^{o}C. The phase changes of PSCFN sample in H_2 and CH_4 are shown in Fig. 8 (b) and (c), respectively. In Fig. 8(b), it can be seen that the main phase is converted to K_2NiF_4 structure identified as $SrPrFeO_4$ (PDF-# 32-1237) in the I4/m space group from cubic structure of PSCFN (PDF-# 46-0335) in the Pm/3m space group, and some new phase identified as Pr_2O_3 (PDF-# 47-1111) and CoFe-alloy (PDF-# 49-1567/ -1568) appear after PSCFN is reduced in dry H_2 at 900 ^{o}C. It is interesting to find that the K_2NiF_4 structure $SrPrFeO_4$ can be transferred to a pure cubic structure of PSCFN again by treating it in air at 900 ^{o}C, as shown in the Fig. 8(b). XRD pattern of the powder after re-oxidation in air at 900 ^{o}C shows a pure PSCFN phase without any impurity phase in the XRD detector limitation, indicating that PSCFN has good redox recycle stability. From Fig. 8(c), one can see that the intensity of XRD patterns decreases slightly after sintered in CH_4 when comparing with the sample reduced in H_2, indicating that the carbon species on PSCFN shows no additional peak.

Fig. 9 (a) and (b) show the SEM images of NiO-YSZ and PSCFN fresh powders after prepared in air, respectively. One can see that the particle size of Ni is about 0.7 μm (Fig. S2), and the PSCFN particle size is about 0.2-0.6 μm. SEM images of Ni-YSZ and PSCFN after reduced in H_2 at 900 ^{o}C are shown in Fig. 9 (c) and (d), respectively. For Ni-YSZ sample, as shown in Fig. 9(c), the grain sizes of Ni particles are increased to 3-4 mm after reduced in H_2, owe to the easier sintering of Ni particles at high temperature. From Fig. 9(d), one can see that the smooth surface of PSCFN grain changes

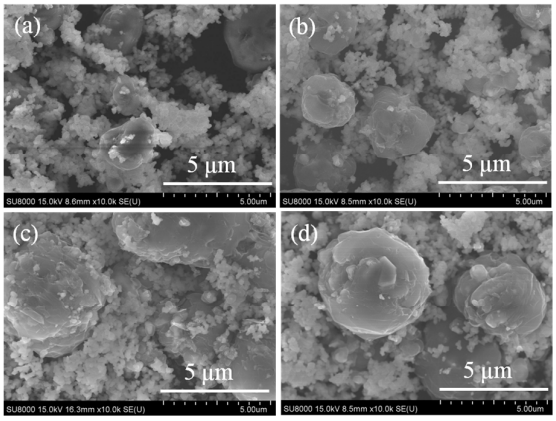

Fig. 10 Typical SEM images of Ni-YSZ samples after exposed to pure CH_4 at (a) 700 ^{o}C, (b) 800 ^{o}C, (c) 850 ^{o}C and (d) 900 ^{o}C.

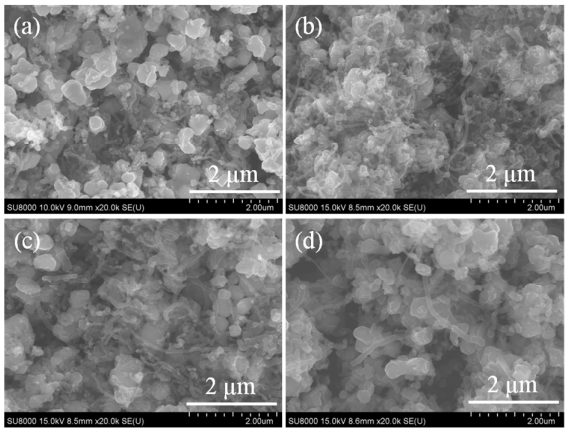

Fig. 11 Typical SEM images of PSCFN samples after exposed to pure CH_4 at (a) 700 ^{o}C, (b) 800 ^{o}C, (c) 850 ^{o}C and (d) 900 ^{o}C.

to homogeneous nano-particle occupied surface. Fig. 9(e) and (f) show SEM images of Ni-YSZ and PSCFN samples after TPO tests in O_2, respectively. One can see that the NiO particle size is similar as the Ni particles shown in Fig. 9(c) and Fig. S4 for Ni-YSZ samples. In contrast, for the PSCFN sample, the re-oxidized sample presents almost the same morphology as that of the original one, indicating the good redox stability of PSCFN sample.

SEM images with carbon deposited at 700, 800, 850 and 900 ^{o}C on Ni-YSZ and PSCFN samples are shown in Figs. 10 and 11, respectively. As shown in Fig. 10, the similar carbon particles are observed in all Ni-YSZ samples. However, the carbon fibres are observed for all PSCFN samples, as shown in Fig. 11 and Fig. S5. The shapes of the deposited carbon may depend on the catalyst properties. For the Ni-YSZ sample, owing to the easier sintering of Ni, the particle size of the Ni increases and the spherical carbon is more easily formed. In contrast, for the PSCFN sample, the nano-sized CoFe-alloy is generated after reduced in H_2 and especially, the sizes of CoFe-alloy are very homogeneous and fine, which could be benefit for the formation of carbon fibres. As shown in Figs. 10 and 11, the only difference between the samples at different

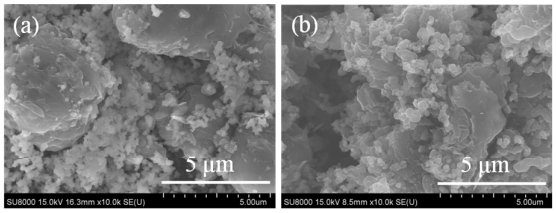

Fig. 12 Typical SEM images of the Ni-YSZ after exposed to CH_4 at 850 ^oC for 30 min (a) and 600 min.

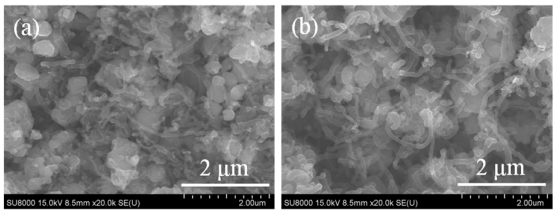

Fig. 13 Typical SEM images of the PSCFN after exposed to CH_4 at 850 ^oC for 30 min (a) and 600 min.

temperatures is the deposited carbon amount. For the Ni-YSZ sample, the carbon particle size increases with the increase in the temperature from 700 to 850 ^oC, and then it becomes similar at 850 and 900 ^oC. However, for the PSCFN sample, the carbon fibres increase with the increase in the temperature from 700 to 800^oC, and then decrease by further increase of the temperature up to 900 ^oC, which is consistent with the results of the CH_4-TPCR at different temperatures, as shown in Fig. 2. Figs. 12 and 13 show the typical SEM images of carbon deposited on Ni-YSZ and PSCFN in CH_4 at 850 ^oC for 30 and 600 min on, respectively. As shown in Fig. 12, the amount of carbon deposited on Ni-YSZ sample for 600 min is much more than that for 30 min, and the carbon particles are connected together. In contrast, for the PSCFN sample, it can be seen that the quantity of carbon fibers, as shown in Fig. 13 (a) and (b), are almost the same, which is in accordance with the behaviours as in Fig. 7.

Conclusions

In summary, the CH_4 temperature-programmed decomposition results revealed that CH_4 decomposition and carbon deposition occurred on PSCFN sample when it was heat-treated in dry CH_4 at higher than 580 ^oC. Comparing with Ni-YSZ sample, the PSCFN showed higher catalytic activity for the cracking CH_4 as well as for the oxidation of cracking products from the temperature-programmed oxidation analysis. The carbon nano-fibers were formed on PSCFN, which is different with the large spherical carbon on Ni-YSZ at the same operation temperature. The property of high catalytic activity for the cracking CH_4 and the oxidation of the generated carbon species on PSCFN could be the main reason for its high performance and stability in direct CH_4 fuel SOFC.

Acknowledgements

This study was supported by Aomori City Government, Japan. P. Zhang gratefully acknowledges the scholarship from the State Scholarship Fund of China Scholarship Council (2012) and Deni S. Khaerudini gratefully acknowledges the scholarship from the Ministry of Education, Culture, Sports, Science and Technology (MEXT) of Japan.

Notes and references

1 A. Boudghene Stambouli, E. Traversa, *Renew. Sust. Energ. Rev.*, 2002, **6,** 433.
2 E. D. Wachsman, Craig A. Marlowe and Kang Taek Lee, *Energ. Environ. Sci.,* 2012, **5,** 5498.
3 W. Wang, C. Su, Y. Wu, R. Ran, Z. Shao, *Chem. Rev.*, 2013, **113,** 8104.
4 Y. M. Guo, G. Largiller, C. Guizard, C. Tardivat, D. Farrusseng, *J. Mater. Chem. A,* 2015, **3,** 2684.
5 X. Ge, S. Chan, Q. Liu, Q. Sun, *Adv. Energy Mater.*, 2012, **2,** 1156.
6 S. Islam, J. M. Hill, *J. Mater. Chem. A,* 2014, **2,** 1922.
7 S. Mclntosh, R. J. Gorte, *Chem. Rev.*, 2004, **104,** 4845.
8 J. Koh, Y. Yoo, J. Park, H. Lim, *Solid State Ionics*, 2002, **149,** 157.
9 D. Yoon, A. Manthiram, *J. Mater. Chem. A,* 2014, **2,** 17041.
10 H. Kim, C. Lu, W. L. Worrell, J. M. Vohs, R. J. Gorte, *J. Electrochem. Soc.*, 2002, **149 (3),** A247.
11 J. Myung, S. Kim. T. H. Shin, D. Lee, J. T. S. Irvine, J. Moon, S. Hyun, *J. Mater. Chem. A,* 2015, **3,** 13801.
12 M. Mogensen, K. Kammer, *Annu. Rev. Mater. Res.,* 2003, **33,** 321.
13 E.P. Murray, T. Tsai, S.A. Barnett, *Nature*, 1999, **400,** 649.
14 S. Park, J.M. Vohs, R.J. Gorte. *Nature, 2000,* **404,** 265.
15 Y. Huang, R. I. Dass, Z. Xing, J. B. Goodenough, *Science,* 2006, **312,** 254.
16 J. C. Fisher II, S. S.C. Chuang, *Catal. Commun.*, 2009, **10,** 772.
17 Y. Sun, J. Li, S. Cui, K. T. C., J. Luo, *Electrochim. Acta,* 2015, **151,** 81.
18 R.J. Gorte, J. M. Vohs, *Annu. Rev. Chem. Biomol.,* 2011, **2,** 9.
19 T. Chen, W. Wang, H. Miao, T. Li, C. Xu, *J. Power Sources,* 2011, **196(5),** 2461.
20 G. Chen, G. Guan, Y. Kasai, H. You, A. Abudula, *J. Power Sources*, 2011, **196,** 6022.
21 S. W. Tao, J. T. S. Irvine, J. A. Kilner, *Adv. Mater.,* 2005, **17(14),** 1734.
22 J. M. Haag, S. A. Barnett, James W. Richardson, Kenneth R. Poeppelmeier, *Chem. Mater.*, 2010, **22(10),** 3283.
23 N. Danilovic, A. Vincent, J. Luo, K. T Chuang, R. Hui, A. R. Sanger, *Chem. Mater.,* 2010, **22(3),** 957.
24 C. Yang, Z. Yang, C. Jin, G. Xiao, F. Chen, M. Han, *Adv. Mater.,* 2012, **24(11),** 1439.
25 P. Zhang, G. Guan, D. S. Khaerudini, X. Hao, M. Han, Y. Kasai, K. Sasagawa, A. Abudula, *J. Power Sources,* 2014, **248,** 163.
26 C. Yang, J. Li, Y. Lin, J. Liu, F. Chen, M. Liu, *Nano Energy,* 2015, **11,** 704.
27 M. Kogler, E.M. Kock, L Perfler, T. Bielz, M. Stoger-Pollach, W. Hetaba, M. Willinger, X. Huang, M. Schuster, B. Klotzer, S. Penner, *Chem. Mater.*, 2014, **26,** 1690.
28 W. Wang, C. Su, Y. Wu, R. Ran, Z. Shao, *J. Power Sources,* 2010, **195,** 402.
29 I. S. Metcalfe, R. T. Baker, *Catal. Today*, 1996, **27,** 285.

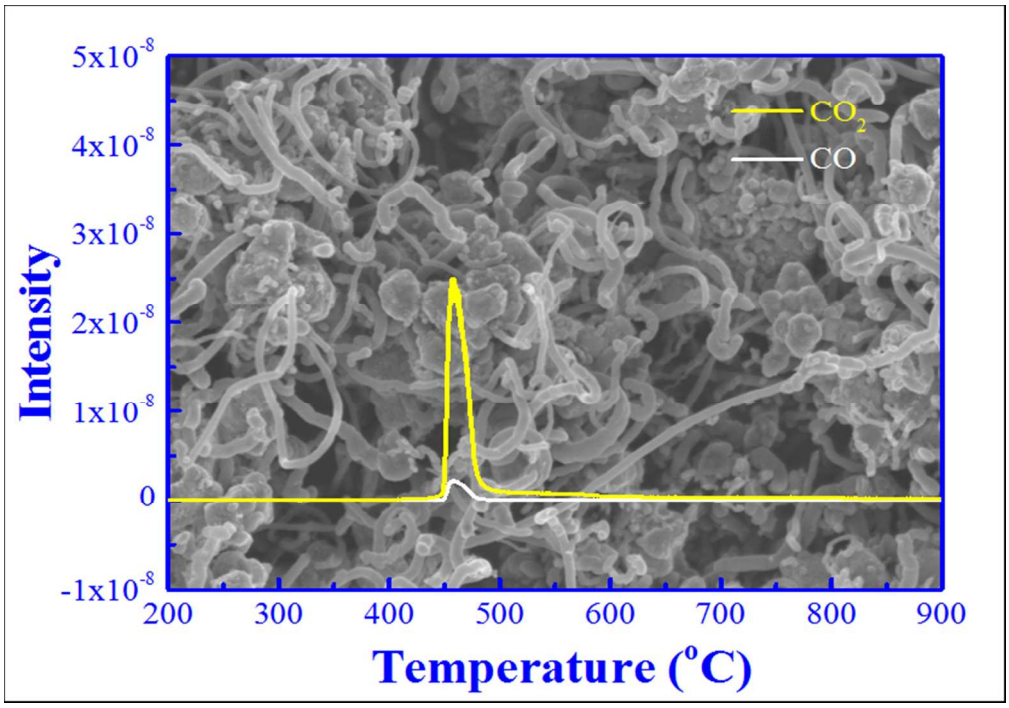

219x152mm (96 x 96 DPI)